Non-canonical histone H3.3 and its chaperones HIRA and DAXX participate in the regulation of KSHV latency

Sarah McMahon[1,3†], Vaibhav Jain[1†], Viacheslav Morozov[2†], Sunantha Sethuraman[1], Jianhong Hu[1], Ritu Shekhar[1], Netanya Keil[1,4], Peter Turner[1], Alexander Ishov[2,3,4*] and Rolf Renne[1,3,4*]

[1]Department of Molecular Genetics and Microbiology, University of Florida, Gainesville, Florida, USA

[2]Department of Anatomy and Cell Biology, University of Florida, Gainesville, Florida, USA

[3]UF Health Cancer Institute, University of Florida, Gainesville, Florida, USA

[4]UF Genetics Institute, University of Florida, Gainesville, Florida, USA

[†]These authors contributed equally to this work

*Corresponding authors

Rolf Renne, rrenne@ufl.edu (RR)

Alexander Ishov, ishov@ufl.edu (AI)

Abstract

Kaposi's sarcoma-associated herpesvirus (KSHV), also named HHV-8, is the etiological agent of Kaposi sarcoma (KS), Primary effusion lymphoma (PEL), and Multicentric Castleman's disease. After de novo infection, KSHV genomes rapidly circularize and acquire a chromatin state that favors latency. During latency, the KSHV episome is decorated with distinct epigenetic marks that segregate the viral genome into transcriptionally active and repressed domains, enabling persistent silencing of lytic genes while retaining the capacity for reactivation. Transcription activity of chromatin is regulated at multiple levels, including the incorporation of histone variants such as H3.3, by a specific set of histone chaperones such as HIRA and DAXX. The interaction between LANA and these interphase active chaperones suggests that H3.3 deposition is a critical driver of early chromatinization and the long-term stability of KSHV latency. We detected rapid H3.3 deposition on KSHV episomes and on episomes within long-term infected cells. Moreover, we demonstrated that genetically disrupting the host H3.3 chaperone HIRA pathway by CRISPR/Cas9-mediated knockout impacted the regulation of LANA and maintenance of viral latency that was not altered in DAXX knockout cells. Collectively, these results support a role for HIRA-mediated H3.3 deposition in the regulation of KSHV latency.

Keywords: KSHV, H3.3, latency, Histone chaperones

52 **Introduction**

53 Kaposi's sarcoma-associated herpesvirus (KSHV) is the causative agent of several
54 human cancers including Kaposi sarcoma (KS)[1] and the lymphoproliferative diseases:
55 Primary effusion lymphoma (PEL)[2] and Multicentric Castleman's Disease (MCD)[3]. A
56 characteristic feature of KSHV pathogenesis is the predominance of a latently infected
57 cell state where long-term persistence supports tumorigenesis. Upon infection of host
58 cells, the KSHV genome is rapidly packaged into chromatin (episomes), utilizing host
59 chromatin machinery that partitions the genome into transcriptionally active and
60 repressed domains[4]. This process is essential for sustained expression of a subset of
61 latency genes, including the Latency Associated Nuclear Antigen (LANA). Upon
62 establishment of viral latency, replication and segregation of viral genomes is essential
63 for long-term viral persistence.

64 The regulation of latency expression is dictated by several processes, including
65 modulation of host histone[5]. Eukaryotic cells express three types of histone H3 variants:
66 H3.1, H3.2, and H3.3[6]. Histone H3.1 and H3.2 are the predominant ("canonical")
67 variants that are expressed solely during S phase of the cell cycle and are exclusively
68 incorporated into newly synthesized DNA[7-9]. The variant histone H3.3 differs from H3.1
69 by only five amino acids, and is highly conserved in mammals[10]. Comparable to
70 canonical H3.1 and H3.2, H3.3 histone tails also undergo epigenetic and biochemical
71 changes[11, 12]. However, unlike the canonical H3.1, histone H3.3 is expressed throughout
72 the cell cycle, can be assembled into chromatin outside of S-phase[13], and is mostly
73 enriched in regions with elevated transcriptional activity[14]. In accord with their availability
74 throughout the cell cycle, histone H3.3 is deposited by unique chaperone complexes,

75 including the histone cell cycle regulator A (HIRA) and death-domain associated protein
76 (DAXX) complexes. HIRA is responsible for deposition of H3.3 into regions of
77 transcriptional activity, nucleosome-free regions, and at sites of DNA damage [14-17].
78 Conversely, DAXX, a PML Nuclear Bodies/ND10-associated protein, is more commonly
79 associated with transcriptionally repressed heterochromatin where it deposits H3.3 to
80 specific transcription factor binding sites, pericentromeric regions, and telomeres [16, 18-20].

81 Evidence suggests that large double-stranded DNA viruses, such as KSHV and
82 EBV, utilize alternative histones and their chaperones during *de novo* viral infection[21].
83 For EBV, it has been shown that the tegument protein BNRF1 suppresses ATRX-DAXX-
84 mediated H3.3 loading onto viral episomes early after infection[22]. KSHV LANA interacts
85 with HIRA, DAXX, and DEK, which all function as H3.3 chaperones[23-25]. LANA also
86 interacts with core components of the HIRA complex and with downstream effectors
87 including the FACT chromatin remodeling complex[25, 26]. Moreover, it has been shown
88 that the recruitment of the Polycomb Repressive Complex-2 (PRC2) complex on
89 epigenetically bivalent and transcriptionally poised promoters is mediated by HIRA-
90 dependent incorporation of H3.3[27]. DAXX was also identified from a proteomic screen
91 as an interactor of LANA[25], and this interaction was recently demonstrated to be critical
92 for epigenetic maintenance of episomes associated with LANA nuclear bodies during
93 KSHV latency[28]. However, whether the enrichment of alternate histone H3.3, mediated
94 by the chaperones HIRA and DAXX, is involved in the establishment and maintenance
95 of latent KSHV episomes has not been established.

96 Here, we tested the hypothesis that the histone variant H3.3 contributes to the
97 establishment and maintenance of KSHV latency. We report that H3.3 is enriched on

98 the latent KSHV genome in PEL BCBL-1 cells and latently infected HEp-2 cells and is
99 deposited on the viral episome during early stages of latency establishment. We further
100 show that the H3.3 histone chaperones HIRA and DAXX colocalize with LANA on KSHV
101 episomes independently of PML/ND10. Using knockout cell lines, we demonstrate that
102 HIRA, but not DAXX, regulates H3.3 positioning within the major viral latency region
103 encompassing LANA. Together, these findings support a role for the H3.3 pathway,
104 particularly HIRA-mediated activity, in the establishment and maintenance of KSHV
105 latency.

106 **Results**

107 **Histone H3.3 is deposited during the pre-latency phase after *de novo* infection.**
108 During *de novo* infection, KSHV releases naked linear DNA into the nucleus of host
109 cells where it circularizes to form viral episomes. The chromatinization of KSHV
110 episomes has been demonstrated as early as two hours post-infection[19, 29]. To test
111 whether H3.3 contributes to early chromatinization, we infected SLK cells with
112 recombinant KSHV/BAC16 and examined H3.3 deposition by ChIP-qPCR on multiple
113 viral promoters at 2, 8, 24, 48, and 72 hrs post infection (Figure 1A). H3.3 deposition
114 was detectable on the RTA promoter and late gene ORF19 promoter at 2 hrs post
115 infection, whereas LANA showed no H3.3 enrichment at this earliest timepoint. At 8 and
116 24 hrs post infection, H3.3 was detected on the RTA promoter and early gene K7
117 promoter, which are known to harbor bivalent marks, and to a lesser extent the ORF19
118 promoter. At late time points (48 and 72 hrs), H3.3 association with the LANA promoter
119 increased while its association with the lytic promoter declined. These data are
120 consistent with early work by others showing that both the RTA and LANA genes are

121 transcribed very early, but that the RTA gene is subsequently silenced in response to
122 increased LANA expression[30].
123 Collectively, these data indicate that H3.3 incorporation is an early and dynamic feature
124 of KSHV episome chromatinization that supports latency establishment.

125 **H3.3 is present on latent viral episomes.**

126 After establishing H3.3 deposition and its chaperones are active during KSHV infection
127 of SLK cells, we wanted to test whether H3.3 is also present on KSHV episomes in
128 infected lymphoid cells. H3.1 and H3.3 only differ by five amino acids, therefore making
129 it difficult to raise an antibody that specifically differentiates these two histone
130 molecules. Therefore, to investigate the presence of histone H3.3 on the KSHV
131 episome, we engineered patient-derived BCBL-1 cells to ectopically express either HA-
132 tagged canonical H3.1 or H3.3 by stable lentivirus transduction and verified HA-H3.1
133 and HA-H3.3 expression by western blot (Supplementary Figure 1). We performed
134 ChIP-seq to map ectopically expressed H3.1 and H3.3 (anti-HA) and LANA to examine
135 their distributions across the KSHV episome (Figure 1B). LANA is enriched on several
136 viral loci, including the KSHV latency-associated region (KLAR), viral Interferon
137 Regulatory Factors (vIRFs), and the lytic switch gene RTA. Canonical histone H3.1 was
138 detected broadly and relatively uniformly throughout the viral genome, whereas histone
139 H3.3 localized as discrete peaks. Except for a cluster of H3.3 peaks spanning the
140 ORF11 to ORF2 region (16.5 kb-18.7 kb), the majority of H3.3 peaks colocalize with
141 LANA binding sites. This co-occupancy of H3.3 and LANA and the association between
142 LANA and the H3.3 chaperone pathways suggest a possible role for LANA in H3.3
143 deposition. To validate these findings on endogenous histones of infected cells, we

144 performed ChIP-qPCR in parental BCBL-1 cells using a H3.3-S31P-specific antibody.
145 The promoters of LANA, K7, and the ORF19 gene were all enriched for endogenous
146 H3.3 (Supplementary Figure 1). Together these data demonstrate that latent KSHV
147 episomes are decorated with H3.3 at multiple loci and H3.3 and LANA show co-
148 occupancy on the viral episome.

149 **H3.3 chaperones HIRA and DAXX interact with and colocalize to LANA speckles in**
150 **KSHV infected cells.**

151 Previous studies have identified LANA to be associated with the H3.3 chaperones HIRA
152 and DAXX[25, 28, 31]. Both chaperones are known to be involved in host immune response
153 to foreign DNA[21] and in remodeling PML/ND10 nuclear bodies[32-38]. KSHV/LANA form
154 unique nuclear speckles to support viral latency and given the interaction of LANA with
155 H3.3 histone chaperones we asked whether DAXX and HIRA affect LANA speckle
156 organization. First, we validated the interaction of KSHV LANA with DAXX and HIRA by
157 coimmunoprecipitation with exogenous overexpression of LANA with either DAXX or
158 HIRA. This demonstrated that both DAXX and HIRA interact with LANA (Figure 2A). To
159 determine whether these interactions reflect spatial proximity in infected cells, we
160 performed immunofluorescence assays (IFA) to compare the localization of LANA,
161 HIRA, DAXX, and PML/ND10 components (Figure 2B). In mock-infected cells, DAXX
162 localized to discrete nuclear bodies that overlapped extensively with PML/ND10
163 (Figures 2Bi-2Biv), whereas HIRA displayed a diffuse nuclear distribution with only
164 limited association with PML bodies (Figures 2Bv-2Bviii). Cells infected with KSHV
165 displayed characteristic LANA nuclear speckles[39] (Figures 2Bix and 2Bxiii) that are
166 spatially distinct from PML/ND10[19]. Interestingly, in KSHV-infected cells, DAXX

167 colocalizes with PML as in uninfected cells, while a portion of DAXX is redistributed and
168 colocalizes with LANA, outside of PML/ND10 (Figures 2Bix – 2Bxii). HIRA also showed
169 pronounced colocalization with LANA speckles in infected cells, independent of
170 PML/ND10 (Figures 2Bxiii – 2Bxvi). Overall, these data demonstrate that in KSHV
171 infected cells both H3.3 chaperones DAXX and HIRA accumulate with KSHV LANA
172 outside of PML/ND10 and that KSHV infection does not affect PML/ND10 structures.

173 Given the association of LANA with H3.3 loading on viral genomes and
174 colocalization of LANA with the histone chaperones DAXX and HIRA, we were
175 interested in dissecting the genetic relationship between LANA and these H3.3
176 chaperones. A panel of LANA domain constructs previously described[40] were used for
177 coimmunoprecipitation experiments with epitope tagged HIRA and DAXX constructs
178 (Supplementary Figure 2A). No specific domain was identified as required for binding,
179 instead interactions with both HIRA and DAXX were strongest when the large,
180 intrinsically disordered region of LANA was present. These results posture that LANA-
181 chaperone association is mediated by multivalent contacts characteristic of proteins that
182 participate in bimolecular condensates[41].

183 **CRISPR/Cas9-based knockout of H3.3 chaperones does not affect LANA speckles**
184 **in latently infected cells.**

185 Given widespread H3.3 loading across the KSHV genome and the interaction and
186 colocalization of DAXX and HIRA with LANA speckles, we next tested the genetic
187 contribution of each H3.3 chaperone pathway to viral latency maintenance. Using
188 CRISPR/Cas9-based gene editing[42, 43] in HEp-2 larynx carcinoma cells we generated
189 DAXX and HIRA knockout (KO) cell lines and introduced a FLAG tag into one of the

190 endogenous H3.3 genes (H3FB) to circumvent specificity limitations of commercially
191 available H3.3 antibodies. Clones were validated by western blot for expression of
192 DAXX, HIRA, and FLAG-H3.3, confirming expression of the knock-in FLAG-H3.3 allele
193 and lack of expression of DAXX and HIRA in the appropriate KO cells (Supplementary
194 Figure 3A). For downstream experiments, one clone of CRISPR control and two clones
195 of each of the HIRA KO and DAXX KO were used. The FLAG-H3.3 knock-in was
196 characterized by IFA and metaphase spreads, confirming chromosome association of
197 FLAG-H3.3 (Supplementary Figure 3B top and middle rows). Lastly, in KSHV infected
198 cells FLAG-H3.3 was diffuse throughout nuclei with intact nuclear LANA speckles
199 (Supplementary Figure 3B bottom row).

200 To examine the localization of DAXX, HIRA, and LANA in these KO KSHV
201 infected lines, we performed IFA in these HEp-2 lines (Figure 3). In control KSHV
202 infected cells, DAXX closely associated with LANA speckles (Figure 3A-D), and HIRA
203 colocalized with LANA (Figure 3E-H) consistent with observations in iSLK cells (Figure
204 2). In HIRA KO cells, HIRA signal is absent and does not affect DAXX/LANA
205 colocalization (Figure 3I-L). However, it is interesting to note that compared to control
206 cells where DAXX is highly localized in LANA speckles (Figure 3B), in HIRA KO cells
207 while some LANA-DAXX interactions are maintained, DAXX is more diffusely distributed
208 within the cell independent of LANA (Figure 3J). Previous studies have shown that upon
209 lytic induction of latently infected cells that DAXX is evicted from LANA speckles[28],
210 perhaps suggesting that HIRA KO cells might support viral episomes more permissive
211 to a lytic state. Additionally, neither PML/ND10 or LANA speckles are affected by HIRA
212 KO (Figure 3M-P). In KSHV infected DAXX KO cells, DAXX staining is absent (Figure

213 3Q-T), and no changes in HIRA association with or formation of PML/ND10 or LANA
214 speckles was identified (Figure 3U-X). Overall, the loss of one of the H3.3 chaperones
215 did not affect the colocalization of the remaining chaperone with LANA and did not
216 perturb PML/ND10 architecture.

217 **HIRA and DAXX are both utilized to load H3.3 onto KSHV episomes.**

218 HIRA and DAXX deposit histone H3.3 into transcriptionally active and repressive
219 chromatin, respectively, but their roles during KSHV latency are not well defined. To
220 map the HIRA- and DAXX-dependent histone H3.3 deposition on latent viral genomes,
221 we performed CUT&RUN in latently infected cells[44]. First, we compared H3.3
222 distribution on the KSHV episome between PEL BCBL-1 cells and HEp-2 latently
223 infected cells. Overall, both cell types show similar, ubiquitous H3.3 loading across the
224 viral genome (Figure 4A). Minor differences in peak patterns were observed at a few
225 loci that may reflect biologically meaningful variation between cell types or arise due to
226 technical differences between ChIP-seq and CUT&RUN or from ectopic versus
227 endogenous H3.3 expression.

228 We next wanted to determine whether H3.3 chaperone deletion could alter H3.3
229 loading onto the viral episome. We compared CUT&RUN from control, HIRA KO, and
230 DAXX KO cells with an antibody to FLAG-tagged H3.3 (Figure 4B). During data
231 processing, we detected selection biases for smaller episomes in some samples
232 (Supplementary Figure 4A), a phenomenon reported previously in infected cells[24, 45].
233 Therefore, to overcome this artifact we examined the signal across sequenced input
234 DNA. From this we identified a large region on the left side of genomes that was
235 particularly reduced in control and DAXX KO samples. Therefore, a scale factor was

236 generated for all samples to scale the left side of genomes to right (Supplementary
237 Figure 4B).

238 After adjustment, we compared FLAG-H3.3 loading between control, HIRA KO,
239 and DAXX KO cells (Figure 4B). Overall, we observed H3.3 loading all along the viral
240 genome independent of genotype. Unexpectedly, we identified that in the region coding
241 for LANA there was an increased signal unique to HIRA KO cells when compared to
242 control and DAXX KO (Figure 4B, zoom in). In addition to H3.3 loading, we also profiled
243 active (H3K4me3) and repressive (H3K37me3) histone modifications across control and
244 KO samples to see if whether these histone chaperones regulate the partitioning the
245 episome into transcriptionally active and repressive regions (Figure 4C). Looking at
246 these marks across the viral genome demonstrated there was no major changes to
247 these histone modifications suggesting the impact of these H3.3 chaperones on the viral
248 episome is more important for loading and less on partitioning the genome into
249 transcriptionally active and repressive regions via epigenetic modification of histones.
250 Overall, our findings indicate both HIRA- and DAXX- mediate incorporation of H3.3 onto
251 viral genomes, with exception of the LANA locus that is affected by HIRA KO.

252 **HIRA loss increases H3.3 at the LANA locus and derepresses viral gene**
253 **expression.**

254 The major finding in our characterization of DAXX- and HIRA-dependent loading
255 of H3.3 was a selective increase in H3.3 occupancy across the LANA locus in HIRA KO
256 cells. To test whether this altered H3.3 loading affects viral transcription, we measured
257 expression of LANA, RTA, and ORF19 by RT-qPCR in latently infected control, DAXX
258 KO, and HIRA KO cells. In the uninduced latent state, HIRA KO cells, but not DAXX KO

259 cells, exhibited significantly elevated RTA and ORF19 transcript levels compared to
260 control (Figure 5A). Under sub-optimal induction conditions that are insufficient to drive
261 robust lytic activation, this increased effect is lost, suggesting that loss of HIRA is critical
262 for maintenance of viral latency rather than productive lytic induction. Consistent with
263 RT-qPCR data, infection with the reporter .219 KSHV recombinant virus revealed
264 detectable PAN-promoter driven RFP in uninduced HIRA KO cells (~9 RFP^+ cells per
265 field), a signal that did not appreciably increase under sub-optimal induction (~7 RFP^+
266 cells per field) (Figure 5B). To assess whether these transcriptional changes translate
267 into infectious output, we performed supernatant transfer from uninduced cells onto
268 naïve 293T cells and quantified GFP^+ recipient cells by flow cytometry at 48 hours.
269 Supernatant from control cells produced minimal GFP^+ infection (0.24%), while DAXX
270 KO supernatant showed a modest increase (0.675), and HIRA KO supernatant
271 produced a larger rise (1.01%) (Figure 5C). Together, these results indicate that loss of
272 HIRA alters H3.3 positioning at the LANA locus and weakens latency control, leading to
273 increased expression of lytic transcripts and a modest rise in virus release, without
274 triggering widespread lytic replication.

275 **Discussion**

276 During latent infection, KSHV acquires and maintains a distinct chromatin state
277 by utilizing host epigenetic machinery. Our work provides additional evidence of direct
278 involvement of the non-canonical histone variant H3.3 and its chaperones HIRA and
279 DAXX in the establishment and maintenance of the latent KSHV episome. We show
280 that HIRA and DAXX H3.3 histone chaperones interact with and colocalize with KSHV-
281 LANA in KSHV-infected cells independent of PML/ND10. We also observed that loss of

282 HIRA, but not DAXX, alters H3.3 deposition onto the KSHV episome, altering loading at
283 the major latency locus LANA with consequences on viral gene regulation and latency.

284 Contrary to the canonical histone H3.1 and H3.2 that are deposited solely during
285 DNA replication in S-phase, deposition of histone variant H3.3 occurs throughout
286 interphase and is presumably available during viral infection in a cell-cycle independent
287 manner. Therefore, we hypothesized that deposition of histone H3.3 plays an important
288 role in early steps of latency establishment, since during KSHV infection LANA interacts
289 either directly with both HIRA and DAXX or indirectly with other downstream
290 components of the HIRA pathway such as Spt16[19, 25, 26, 31]. We observed that H3.3 is
291 deposited on KSHV episomes as early as 2 hours after *de novo* infection prior to the
292 establishment of latency and is present during long-term latency. This suggests that the
293 H3.3 pathway is involved early in the process of KSHV latency establishment. However,
294 future analyses using these genetic knockout lines will be important to determine the
295 relative contribution of HIRA and DAXX on H3.3 loading early after *de novo* infection
296 and consequences of latency establishment in the absence of both chaperone proteins.

297 Our studies revealed that both HIRA and DAXX histone chaperones associate
298 with LANA speckles independent of PML/ND10 suggesting that incorporation of these
299 histone chaperones into LANA speckles may support loading of H3.3 histones onto
300 KSHV episomes and regulate viral latency. In HIRA KO cells that we characterize as
301 having a modest defect in latency control, a redistribution of DAXX from LANA speckles
302 was noticed with an increased nuclear diffuse pattern. This is consistent with a previous
303 study that showed that upon lytic reactivation that DAXX is partially evicted from LANA
304 speckles and proposed this as a mechanism to restrict loading of histone onto newly

305 synthesized linear templates[28]. LANA has previously been shown to undergo
306 SUMOylation that facilitates association with transcriptional repressors and that
307 reactivation leads to deSUMOylation through disruption of interactions with SUMO
308 ligases[46]. Our interaction data of LANA domains with DAXX did not identify any specific
309 interaction domains; however, it would be interesting in future studies to examine how
310 differential SUMOylation of LANA may affect the localization and dispersion of DAXX in
311 latency and lytic replication. DAXX harbors two SUMO Interaction Motifs (SIM) that are
312 known to be important for localizing DAXX to nuclear domains including PML/ND10[47, 48].
313 Specifically, SUMOylated interaction partners have been shown to stabilize DAXX
314 retention in PML bodies[49]. Future studies aimed at deciphering the temporal and spatial
315 localization of DAXX to LANA speckles across latency and reactivation will clarify this
316 important protein-protein interaction and implications on epigenetic maintenance of viral
317 episomes.

318 While DAXX and HIRA both load H3.3 onto viral genomes, only loss of HIRA is
319 essential for maintaining viral latency. Our data shows that in the absence of HIRA there
320 is a site-selective effect on H3.3 loading at the major latency locus LANA that results in
321 loss of viral latency. These findings are supported by published studies examining HIRA
322 on DNA virus latency[50]. Previous work looking at the role of HIRA in the context of DNA
323 virus infection or upon transfection of plasmid DNA demonstrated that HIRA was
324 important for packaging foreign DNA into chromatin upon introduction of these foreign
325 DNA into cells. Additionally, these studies demonstrated that in both cell culture and *in*
326 *vivo* infection models that HIRA was critical for restricting lytic gene activation via
327 regulation of host antiviral responses and therefore had higher lytic replication in the

328 context of HIRA knockdown. Here, we also observed that HIRA KO leads to loss of viral
329 latency with concomitant induction of a predominantly unproductive lytic virus
330 replication.

331 In profiling histone modifications (H3K37me3 and H3K4me3), we did not detect
332 broad changes in these modifications in HIRA KO cells, however, loss of HIRA had clear
333 effects on viral gene expression. This suggests that the transcriptional regulation in this
334 context occurs independently of overt remodeling of chromatin and instead may reflect
335 altered H3.3 positioning, changes in transcription factor occupancy, RNA polymerase
336 dynamics or other chromatin modifying events not captured in our analyses.
337 Additionally, unlike previous work which showed reduced H3.3 loading on host or viral
338 genomes with HIRA knockdown[50, 51], our findings had the unexpected consequence of
339 increased loading, however, specifically at the locus for LANA. This could be due to a
340 direct effect of HIRA loss where DAXX is now able to freely load H3.3 at this locus or
341 alternatively an indirect effect on regulation of host or viral factors regulating chromatin
342 dynamics at the major latency locus. Future mechanistic work focused on the direct vs.
343 indirect effects of HIRA on host and KSHV episomes in latency will help resolve the
344 pathway in which loss of HIRA disrupts latency.

345 Taken together, our findings support a model where the H3.3 histone chaperones
346 DAXX and HIRA both participate as machinery in loading H3.3 onto viral episomes. We
347 demonstrate that H3.3 is loaded early after de novo infection (within hours) and is stably
348 maintained on latent episomes, implicating H3.3 as both an early and persistent
349 determinant of viral latency. While we demonstrate that both DAXX and HIRA localize to
350 LANA speckles independent of PML bodies, HIRA has a non-redundant role in

351 maintaining latency via site-selective regulation of H3.3 deposition within the LANA
352 locus, suggesting that HIRA acts as a critical checkpoint for controlling latency via
353 precise spatial H3.3 loading not global H3.3 abundance. Future studies examining how
354 LANA coordinates viral and host pathways to maintain latency will further the
355 understanding of herpesvirus exploitation of host epigenetic machinery to balance viral
356 latency and reactivation.

357 **Materials and Methods**

358 **Cell lines, media, antibodies and virus**

359 BCBL-1 PEL cells were grown in complete RPMI 1640 media[52]. BCBL-1 cells
360 overexpressing histone H3.3 were created by transducing the plasmid pOZ-HA-H3.1 or
361 -H3.3 which couples the expression of histones with the interleukin-2 receptor chain α
362 (IL2Rα), which was used to sort transduced cells. This system, which has been widely
363 used to characterize genome-wide H3.3 occupancy, has also been used successfully to
364 study HSV-1 chromatinization during lytic replication[53].

365 Antibodies used were as follows: DAXX 677B rabbit (in house); DAXX 5.14
366 mouse monoclonal[54]; PML 14 rabbit[55]; and HIRA WC119.2H11 mouse monoclonal
367 (generous gift from Dr. Peter Adams, Sanford Burnham Prebys Medical Discovery
368 Institute). Antibodies for ChIP were control rabbit IgG (Santa Cruz Biotechnology, sc-
369 2027), rat IgG (Santa Cruz Biotechnology, sc-2026), rabbit against H3K4me3 (Abcam,
370 ab8580), H3K27me3 (Upstate, 07-449), rat LANA monoclonal antibody (ABI Inc., LN53),
371 and rabbit anti-Histone H3.3 (phospho S31) antibody (Abcam, ab92628). Virus was

372 produced from iSLK cells as described previously and were used to produce .219 and
373 BAC16 virus [56-58].

374 ***De novo* infections and creation of stably infected cells.**

375 For *de novo* infections in kinetic experiments, cells were infected with BAC16 virus (300
376 virus particles per cell) for 2 hours and then unbound virus removed by PBS washing.
377 Cells were then collected immediately or at post-infection time points as stated and
378 processed for ChIP.

379 For creating stably infected cell lines, cells were infected as described above and
380 selected for greater than two weeks to ensure stable maintenance of BAC16 or .219.
381 The resulting cells were maintained in hygromycin- or puro-containing media for BAC16
382 and .219 respectively.

383 **Coimmunoprecipitation**

384 For coimmunoprecipitation studies, 293T cells were transfected with plasmid constructs
385 using ExtremeGene9 (Roche). After 48 hours cells were lysed in lysis buffer (7.6mM
386 NaH_2PO_4, 12.4mM Na_2HPO_4, 250mM NaCl, 30mM NaPPi, 5mM EDTA, 10mM NaF,
387 0.1% NP-40, pH 7.0, complete protease inhibitor cocktail (Roche)) and quantified using
388 BCA assay. For immunoprecipitation, 1mg of protein was incubated overnight with
389 FLAG M2 magnetic beads (Sigma) diluted in IP buffer (50mM Tris-HCl pH 7.4, 150mM
390 NaCl, 1mM EDTA, 1% Triton-X, complete protease inhibitor cocktail (Roche)). The
391 following day beads were washed with IP buffer and eluted with FLAG peptide (Sigma).

392 **Western blot**

393 Cells were lysed directly in Laemmli buffer. Protein samples were separated by 4-20%
394 SDS-PAGE gels (Biorad), transferred to nitrocellulose membranes (Whatman, Dassel,
395 Germany), and blocked with 5% non-fat milk/PBS, 0.1% Tween (PBST). Primary
396 antibodies were diluted in 5% milk/PBST and incubated overnight at 4°C. Membranes
397 were then washed 3X with PBST and incubated for 1 hour at RT with appropriate
398 secondary antibody at 1:5000. Membranes were then washed 3X with PBST and were
399 visualized by enhanced chemiluminescence (ECL).

400 **Immunofluorescence (IFA)**

401 IFAs were performed as previously described with a few modifications for adherent
402 cells[59]. In brief, cells were grown on glass cover slips in a 24-well plate. Prior to staining
403 cells were washed twice with PBS, fixed with 1% formaldehyde, and permeabilized with
404 PBS 0.2% Triton X-100 buffer. After two more washes, appropriately diluted primary
405 antibody was added and incubated at room temperature for 60 minutes, followed by
406 PBS washes and addition of a fluorescently tagged secondary antibody. Secondary
407 antibody was washed off using PBS and coverslips were mounted on glass slides with
408 media containing DAPI for analysis by microscopy.

409 **Flow cytometry**

410 KSHV BAC16 infected HEp-2 cell supernatant was used for spin-inoculation of 293T
411 supplemented with 10μg/mL polybrene at 2,500rpm for 90 minutes. The next morning
412 virus containing media was removed and after 48 hours cells were fixed, washed in
413 PBS, and resuspended in FACS Buffer (PBS, 2% FBS, 1mM EDTA). Cells were

414 analyzed on the BD Symphony A3 with gating done on uninfected 293T (GFP^-) and
415 293T-BAC16 (GFP^+). Data were analyzed in FlowJo.

416 **Production of HEp-2 cells with FLAG-tagged H3F3B gene, DAXX and HIRA**
417 **knockouts.**

418 HEp-2 cells were electroporated using the Neon Transfection system (Invitrogen) with
419 equimolar amount of the crRNA/tracrRNA (Integrated DNA Technologies) targeting 5'-
420 terminus of the H3F3B gene, the single-stranded oligonucleotide donor template
421 containing the FLAG sequence and the Alt-R S.p. Cas9 nuclease (Integrated DNA
422 Technologies). After 3 days cells were seeded 1 cell/well into 96-well plates for clonal
423 growth. Clones were screened by immunofluorescence with FLAG antibodies. The
424 correct knock-in of the FLAG tag into H3F3B gene was confirmed by DNA sequencing.
425 DAXX and HIRA knockouts in HEp-2 cells were produced as previously described[51].

426 **mRNA analysis using qPCR**

427 WT BAC16 virus infected control, HIRA KO, and DAXX KO cells were seeded in a 6-
428 well plate in triplicate. The cells either remained untreated or were treated with inducer
429 (2 mM sodium butyrate) and were incubated at 37ºC for 48 hours. The cells were
430 washed with PBS, and RNA was isolated by using the previously described RNA-Bee
431 protocol[60]. DNase digestion of RNA was performed using the Turbo DNase kit from
432 Ambion (AM 2238). RNA was then converted to cDNA using the ABI High-Capacity RNA
433 to cDNA kit. The cDNA was analyzed using the ABI StepOne or Roche LightCycler
434 System for the expression of the latent gene LANA, lytic switch gene RTA, and the late
435 genes ORF19 and ORF59 using SYBR green chemistry.

436 **Chromatin Immunoprecipitation (ChIP)**

437 ChIP-seq was performed to assess LANA, H3.1 and H3.3 binding on the KSHV genome
438 in BCBL-1 cells, and to assay H3K4me3 (activating) and H3K27me3 (repressive)
439 epigenetic marks. The kinetics of H3.3 deposition on the KSHV epigenome post de
440 novo infection of SLK cells were measured by ChIP-qPCR. For ChIP-seq, 10 million
441 cells and for ChIP qPCR following de novo infection, 100,000 cells per antibody were
442 used in triplicate for chromatin preparation. Cells were washed with PBS (room
443 temperature), fixed with 1% formaldehyde in the plate for 10 min at room temperature
444 followed by quenching of formaldehyde by adding 2.5 M glycine to a final concentration
445 of 0.125 M. Cells were washed twice with PBS, and 10 mL ice cold Farnham lysis buffer
446 (5 mM PIPES [pH 8.0], 85 mM KCl, 0.5% NP-40) with protease inhibitors was added to
447 the plate. Cells were scraped off mechanically and centrifuged at 3000 rpm for 5 min at
448 4ºC. Cells were further incubated in Farnham lysis buffer on a rocking platform for 5 min
449 and were pelleted. The nuclei thus obtained were resuspended in 160 µL RIPA buffer
450 (1% NP-40, 0.5% sodium deoxycholate, in 1×PBS with protease inhibitor). For 293T
451 cells, 0.3% SDS was used, and for iSLK cells 0.7% SDS. The chromatin was sheared
452 for a peak enrichment of approximately 300 bp in a Diagenode Bioruptor for SLK with
453 settings power output H; three times 5 min each (0.5% SDS RIPA) and one-time M
454 output for 5 min. For BCBL-1 cells (0.3% SDS RIPA) Power output H; two times 5 min
455 each. The chromatin was obtained by centrifugation of the cells at 14000 RPM for 15
456 min at 4ºC. The obtained chromatin was diluted with the RIPA buffer to adjust the final
457 SDS concentration to 0.1%. Antibodies (5 µg/10 million cells) of interest were
458 subsequently added. Antibody and chromatin complex was incubated overnight at 4ºC.

459 The complex was then subjected to binding with pre-washed 20 µl Pierce protein A/G
460 magnetic beads (88802) (PBS 10% BSA). The bead, antibody and chromatin complex
461 was incubated in cold room for another two hours. Magnetic separation was performed
462 to collect the beads. Beads were washed five times with 1 mL LiCl wash buffer with
463 protease inhibitor and once with TE. The DNA was reverse-crosslinked by incubating
464 twice in 150 µL elution buffer. DNA was isolated by using Monarch PCR purification kit
465 and resuspending in 50 µL water. For qPCR, 1 µL was used per 10 µL reaction and
466 either IgG or input was used for quantification and control.

467 **ChIP Sequencing**

468 ChIP libraries were created using NEB Ultra II kit (E7645S) for Illumina as per the
469 manufacturer's recommendations. The sequencing was performed by multiplexing the
470 libraries on HiSeq 3000 platform using 1*150 runs at the University of Florida ICBR.

471 The subtle differences in chromatin modifications were observed by performing
472 normalization strategies using Drosophila chromatin spike-in strategies with some
473 modifications[61]. We utilized Active Motif "spike-in" control chromatin and antibody
474 (61686 and 53083) kits. Before performing the ChIP, the chromatin from 10 million cells
475 was pre-mixed with 50 ng "spike-in" control chromatin made from Schneider's
476 Drosophila Line 2 (S2) cells and 2 µg per 10 million cells of Drosophila-specific histone
477 variant, H2Av antibody. 4 µg specific antibody of interest was then added to perform
478 ChIP as described above.

479 The ChIP-seq was analyzed as follows. Paired-end reads were quality checked
480 using FastQC. Adaptors were trimmed using the Trimmomatic program with the

481 settings, ILLUMINACLIP: adapters.fa:2:30:10, LEADING:3, TRAILING:3 and
482 MINLEN:36. Trimmed reads were independently aligned to the KSHV viral genome
483 (NCBI:GQ994935), the Drosophila genome (dm6), and the human genome (hg19) using
484 bowtie2 retaining only the best alignment for every read. The mapped reads were
485 sorted using samtools and duplicate reads were removed using Picard MarkDuplicates.
486 For the viral and human alignments, ChIP-seq peaks were called using MACS2 with the
487 setting --nomodel and --extsize 147 and without specifying any control samples. To
488 quantitatively scale the peaks on the viral genome, the scaling factor was calculated
489 based on the number of reads that aligned to the spike-in (Drosophila) sample as
490 previously described[61]. To account for differences in viral episome copies between
491 infected WT, DAXX KO, and HIRA KO cells, we calculated an 'episome factor' as the
492 ratio of number of aligned reads in input from control cells (WT) to input from knockout
493 cells (DAXX KO or HIRA KO). The effective scaling factor was the product of spike-in
494 scaling factor and the episome factor. In case of human samples, only the spike-in
495 factor was used as the effective scaling factor. The peaks were scaled using a custom
496 python script. All scaled and unscaled bedgraph (BDG) files were then converted to
497 wiggle (WIG) files for visualization in IGV.

498 **Cleavage Under Targets & Release Using Nuclease (CUT&RUN)**

499 CUT&RUN was used to map FLAG-H3.3 in HEp-2 cells following the Active Motif kit
500 (53180). This protocol leverages the fusion of protein A to micrococcal nuclease (pA-
501 MNase) to selectively cleave antibody-bound chromatin in nuclei of cells that are
502 immobilized on concanavalin (conA) beads. Cleaved fragments are released into the
503 supernatant and collected for library construction and Illumina Sequencing. Antibodies

504 for FLAG (Biolegend) & IgG (Biolegend) were individually added to each sample.
505 Cleaved fragments were library prepped using the NEB Ultra II library preparation kit for
506 Illumina sequencing libraries.

507 **CUT&RUN Data Analysis**

508 Samples were prepared as 150-bp, paired-end barcoded libraries and sequenced on
509 the Illumina NovaSeq 6000 instrument at the University of Florida Interdisciplinary
510 Center for Biotechnology Research (ICBR) NextGen DNA Sequencing Core. Sample
511 quality was analyzed by FastQC and adapter trimming and quality processing by
512 Trimmomatic. Reads were aligned with Bowtie2 to a concatenated, repeat-masked
513 genome of human GRCh38/hg38 and KSHV BAC16 genome (GQ994935.1). Aligned
514 BAM files were used to generate KSHV genome tracks visualized in IGV.

515 Initial analyses of gene tracks for samples indicated a selection for smaller
516 genomes. To normalize for this, samples were scaled based on a scale factor created
517 from sequenced input. Briefly, coverage from input samples were binned (500bp) across
518 the genome to examine read count depth on the left and right side of genome. A scale
519 factor was then generated, and the left end of genomes were scaled to account for
520 enrichment of smaller episomes consistent on the right end of genomes. Scaled KSHV
521 genome tracks were used for FLAG H3.3 visualization in IGV.

522 **Data Availability Statement**

523 All data presented here are available from Gene Expression Omnibus (GEO) under the
524 accession number GSE224343. The accession number will be incorporated in the
525 manuscript when it is available.

Acknowledgements: This project was funded by NCI/P01CA214091 to R.R. and NIDCR R01 DE026707 to R.R./A.I. and support of UFHCI to R.R./A.I. S.M. was supported by NCI T32CA257923. The authors would like to thank the University of Florida Interdisciplinary Center for Biotechnology Research (UF-ICBR) Cytometry Core (RRID:SCR_019119) and Gene Expression and Genotyping Core (RRID: SCR_019145) for their expertise.

Figure Legends

Figure 1. Histone H3.3 is incorporated in the KSHV episome early after de novo infection and in latently infected PEL cells. (A) Kinetic analysis of H3.3 deposition onto latent and lytic promoters after de novo infection. Histone H3.3 occupancy was determined by ChIP-qPCR at the indicated time points after *de novo* infection of SLK cells with KSHV/BAC16. H3.3 ChIP was performed using anti-Histone H3.3 (phospho S31) antibody. Occupancy of the LANA, K7, and RTA promoters, and ORF19 gene body is shown. Enrichment is expressed as fold increase over IgG control. (B) ChIP-seq assays were performed in BCBL-1 cells stably expressing HA-tagged canonical histone H3.1 (HA-H3.1) or HA-tagged histone variant H3.3 (HA-H3.3) using an anti-HA antibody to detect tagged histone. LANA ChIP-seq was performed in BCBL-1 cells with LANA monoclonal antibody. The ChIP-seq peaks for HA-tagged H3.1, H3.3, and LANA are shown aligned to the KSHV genome. The genome track shows KSHV genome organization with genes of interest highlighted latent (LANA – red), immediate early (RTA - yellow), early (K11 - green), and late (ORF19 – cyan).

547 **Figure 2. H3.3 chaperones DAXX and HIRA interact with LANA and colocalize to**
548 **LANA speckles in KSHV-infected SLK cells.** (A) Interaction of LANA with histone
549 chaperones by coimmunoprecipitation of FLAG-LANA with HA-HIRA and GFP-DAXX in
550 293T cells. (B) Top two rows (i - viii): uninfected SLK cells; bottom two rows (ix - xvi):
551 KSHV-infected SLK cells. (i – iv): Localization of DAXX (green) and ND10/PML (blue).
552 (v - viii) HIRA localization (green) in uninfected SLK cells. DAXX colocalizes with
553 ND10/PML NBs (PML), while HIRA has minor accumulation at ND10/PML NBs. Third
554 row (infected SLK cells, ix - xii): DAXX (green) colocalizes with LANA (red) and is
555 associated with ND10/PML NBs (PML, blue). The inset at the bottom right demonstrates
556 the colocalization of DAXX with both LANA and PML. Bottom row (xiii - xvi): HIRA
557 (green) has substantial colocalization with LANA (red), and minor accumulation at
558 ND10/PML NBs (PML, blue).

559 **Figure 3. Characterization of DAXX KO and HIRA KO in KSHV latently infected**
560 **cells. (**A - H) Distribution of H3.3 chaperones DAXX and HIRA in KSHV infected HEp-2
561 cells. Top row (A - D): DAXX (green) colocalizes with LANA (red) and is associated with
562 ND10/PML NBs (PML, blue) in four representative nuclei. The inset at the bottom right
563 demonstrates the colocalization of DAXX with both LANA and PML. Second row (E - H):
564 HIRA (green) has minor colocalization with LANA (red), and ND10/PML NBs (PML,
565 blue). I - P shows the distribution of DAXX and HIRA in KSHV infected HIRA KO HEp-2
566 cells. (I - L): DAXX (green) colocalizes with LANA (red) and is associated with
567 ND10/PML NBs (PML, blue), similar to control HEp-2 cells (in A - D above). HIRA KO
568 does not affect the intranuclear distribution of DAXX. (M – P): No visible HIRA (green);
569 LANA (red), and ND10/PML NBs (PML, blue) are not affected by HIRA KO. (N)

570 Increased diffuse signal of DAXX (green) compared to control (B). Q - X show
571 distribution of DAXX and HIRA in KSHV infected DAXX KO HEp-2 cells. (Q - T): No
572 visible DAXX (green); LANA (red), and ND10/PML NBs (PML, blue) are not affected by
573 DAXX KO. (U – X): HIRA (green) has minor colocalization with LANA (red), and
574 ND10/PML NBs (PML, blue), like control HEp-2 cells (A). DAXX KO does not affect the
575 intranuclear distribution of HIRA.

576 **Figure 4. Histone chaperones DAXX and HIRA both load H3.3 onto KSHV**
577 **episomes.** (A) H3.3 loading across KSHV episome in BCBL1 (ChIP-seq as depicted in
578 Figure 1) and FLAG-tagged H3.3 in HEp-2 cells (CUT&RUN). (B) FLAG H3.3
579 CUT&RUN in wild-type control, DAXX KO, and HIRA KO HEp-2 KSHV infected cells.
580 Lower panel is zoomed in on ORF73 (LANA) locus. (C) ChIP-seq for histone
581 modifications (H3K27me3 and H3K4me3) in wild-type control, DAXX KO, and HIRA KO
582 across viral episomes in HEp-2 KSHV infected cells. For each panel, the genome track
583 shows KSHV genome organization with the following viral latent (LANA – red),
584 immediate early (RTA - yellow), early (K11 - green), and late (ORF19 – cyan) genes
585 highlighted for reference.

586 **Figure 5. HIRA KO disrupts maintenance of viral latency in HEp-2 KSHV infected**
587 **cells.** (A) Wild-type control (CTL), DAXX KO, and HIRA KO HEp-2 cells were infected
588 with KSHV/BAC16 virus, and latently infected cells were selected using hygromycin.
589 Infected cells were either uninduced (panel A; left) or sub-optimally induced with 1 mM
590 sodium butyrate (panel A; right) for 48 hours. Transcripts of LANA, RTA, and ORF19
591 were quantified by RT-qPCR normalized to GAPDH. In uninduced cells, data is
592 represented as relative to CTL. For sub-optimal induction experiments data is

593 represented as relative to respective uninduced expression. Error bars indicate the SD
594 of three biological replicates and significance of p-values are represented by asterisks
595 (*p<0.1, ** p<0.01, ***p<0.001, ****p<0.0001). (B) Wild-type control (CTL), DAXX KO,
596 and HIRA KO HEp-2 cells were infected with KSHV/.219 dual reporter virus. RFP
597 representing lytic activation was examined in uninduced or sub-optimally induced cells
598 and presented as fluorescence images (left) and quantified across multiple fields (right).
599 (C) Supernatant from uninduced control (CTL), DAXX KO, and HIRA KO HEp-2 cells
600 was used to transduce naïve 293T cells and GFP positivity was determined at 24 hours
601 post transduction by flow cytometry.

602 **Supplementary Figure 1. Validation of H3.3 loading in BCBL-1.** (A) BCBL-1 cells
603 were transduced with HA-H3.1- or HA-H3.3-expressing retrovirus and sorted with IL2Ra
604 antibody-conjugated magnetic beads. Lysates were analyzed by western blotting with
605 anti-HA mAb and GAPDH loading control. (B) ChIP-qPCR in BCBL-1 to examine H3.3
606 loading (H3.3-S31P) at viral promoters of LANA, K7, and ORF19.

607 **Supplementary Figure 2. Interaction of H3.3 chaperones with LANA deletion**
608 **constructs.** (A) Schematic of N-terminally FLAG-tagged LANA domain deletions used
609 for coimmunoprecipitation assays. (B) Coimmunoprecipitation assays in 293T of FLAG-
610 tagged LANA domain deletions with HA-tagged HIRA or GFP-tagged DAXX constructs.
611 Expression of constructs is observed from input samples in IP assays.

612 **Supplementary Figure 3. Characterization of DAXX and HIRA knockout and H3.3-**
613 **FLAG knock-in HEp-2 cells.** (A) CRISPR/Cas9 was used to produce DAXX KO and
614 HIRA KO HEp-2 cells with a FLAG knock-in into the endogenous H3.3 locus. The

615 FLAG-encoding sequence was introduced at 5' end of the H3F3B gene by homologous
616 recombination. Single-cell clones were characterized for DAXX and HIRA KO and
617 expression of FLAG-H3.3 using western blot. In control (CTL), HIRA KO, and DAXX KO
618 cells, several clones showing FLAG-H3.3 expression were obtained. WT HEp-2 were
619 used as control. Actin was used as loading control. (B) Microscopy analysis of
620 endogenous tagged FLAG-H3.3. Top: exponentially grown cells; middle: metaphase
621 spread confirming chromosome association of FLAG-H3.3. FLAG (green): DNA (blue).
622 Bottom: Distribution of H3.3 in KSHV infected HEp-2 cells. H3.3 (FLAG, green) has
623 homogenous nuclear distribution in KSHV-infected (LANA, red) HEp-2 cells. DNA: blue.

624 **Supplementary Figure 4. Normalization of FLAG H3.3 signal in CUT&RUN data.** (A)
625 Gene tracks of FLAG H3.3 signal along KSHV genome in control, DAXX KO, and HIRA
626 KO HEp-2 cells by CUT&RUN (B) Distribution of counts by 500bp bins of KSHV
627 genome for CTL, DAXX KO, and HIRA KO cells. Signal breakpoint for smaller episomes
628 was identified and a scale factor was produced as the ratio of the right side of genome
629 to left side of genome that was applied to samples for normalization.

630 **REFERENCES**

631 1. Chang, Y. *et al.* Identification of herpesvirus-like DNA sequences in AIDS-
632 associated Kaposi's sarcoma. *Science* **266**, 1865-1869 (1994).
633 2. Cesarman, E., Chang, Y., Moore, P.S., Said, J.W. & Knowles, D.M. Kaposi's
634 sarcoma-associated herpesvirus-like DNA sequences in AIDS-related body-
635 cavity-based lymphomas. *N Engl J Med* **332**, 1186-1191 (1995).
636 3. Soulier, J. *et al.* Kaposi's sarcoma-associated herpesvirus-like DNA sequences in
637 multicentric Castleman's disease. *Blood* **86**, 1276-1280 (1995).
638 4. Campbell, M., Yang, W.S., Yeh, W.W., Kao, C.H. & Chang, P.C. Epigenetic
639 Regulation of Kaposi's Sarcoma-Associated Herpesvirus Latency. *Front Microbiol*
640 **11**, 850 (2020).
641 5. Lu, F., Stedman, W., Yousef, M., Renne, R. & Lieberman, P.M. Epigenetic
642 regulation of Kaposi's sarcoma-associated herpesvirus latency by virus-encoded

643 microRNAs that target Rta and the cellular Rbl2-DNMT pathway. *J Virol* **84**,
644 2697-2706 (2010).
645 6. Henikoff, S. Nucleosome destabilization in the epigenetic regulation of gene
646 expression. *Nat Rev Genet* **9**, 15-26 (2008).
647 7. Hake, S.B. & Allis, C.D. Histone H3 variants and their potential role in indexing
648 mammalian genomes: the "H3 barcode hypothesis". *Proc Natl Acad Sci U S A*
649 **103**, 6428-6435 (2006).
650 8. Verreault, A., Kaufman, P.D., Kobayashi, R. & Stillman, B. Nucleosome assembly
651 by a complex of CAF-1 and acetylated histones H3/H4. *Cell* **87**, 95-104 (1996).
652 9. Franklin, S.G. & Zweidler, A. Non-allelic variants of histones 2a, 2b and 3 in
653 mammals. *Nature* **266**, 273-275 (1977).
654 10. Thatcher, T.H. & Gorovsky, M.A. Phylogenetic analysis of the core histones H2A,
655 H2B, H3, and H4. *Nucleic Acids Res* **22**, 174-179 (1994).
656 11. Campos, E.I. & Reinberg, D. New chaps in the histone chaperone arena. *Genes*
657 *Dev* **24**, 1334-1338 (2010).
658 12. Mattiroli, F., D'Arcy, S. & Luger, K. The right place at the right time: chaperoning
659 core histone variants. *EMBO Rep* **16**, 1454-1466 (2015).
660 13. Wu, R.S., Tsai, S. & Bonner, W.M. Patterns of histone variant synthesis can
661 distinguish G0 from G1 cells. *Cell* **31**, 367-374 (1982).
662 14. Ray-Gallet, D. *et al.* Dynamics of histone H3 deposition in vivo reveal a
663 nucleosome gap-filling mechanism for H3.3 to maintain chromatin integrity. *Mol*
664 *Cell* **44**, 928-941 (2011).
665 15. Ray-Gallet, D. *et al.* HIRA is critical for a nucleosome assembly pathway
666 independent of DNA synthesis. *Mol Cell* **9**, 1091-1100 (2002).
667 16. Goldberg, A.D. *et al.* Distinct factors control histone variant H3.3 localization at
668 specific genomic regions. *Cell* **140**, 678-691 (2010).
669 17. Zhang, H. *et al.* RPA Interacts with HIRA and Regulates H3.3 Deposition at Gene
670 Regulatory Elements in Mammalian Cells. *Mol Cell* **65**, 272-284 (2017).
671 18. Salomoni, P. The PML-Interacting Protein DAXX: Histone Loading Gets into the
672 Picture. *Front Oncol* **3**, 152 (2013).
673 19. Gunther, T., Schreiner, S., Dobner, T., Tessmer, U. & Grundhoff, A. Influence of
674 ND10 components on epigenetic determinants of early KSHV latency
675 establishment. *PLoS Pathog* **10**, e1004274 (2014).
676 20. Lewis, P.W., Elsaesser, S.J., Noh, K.M., Stadler, S.C. & Allis, C.D. Daxx is an
677 H3.3-specific histone chaperone and cooperates with ATRX in replication-
678 independent chromatin assembly at telomeres. *Proc Natl Acad Sci U S A* **107**,
679 14075-14080 (2010).
680 21. Mai, J., Nazari, M., Stamminger, T. & Schreiner, S. Daxx and HIRA go viral - How
681 chromatin remodeling complexes affect DNA virus infection. *Tumour Virus Res*
682 **19**, 200317 (2025).
683 22. Tsai, K. *et al.* Viral reprogramming of the Daxx histone H3.3 chaperone during
684 early Epstein-Barr virus infection. *J Virol* **88**, 14350-14363 (2014).
685 23. Krithivas, A., Fujimuro, M., Weidner, M., Young, D.B. & Hayward, S.D. Protein
686 interactions targeting the latency-associated nuclear antigen of Kaposi's
687 sarcoma-associated herpesvirus to cell chromosomes. *J Virol* **76**, 11596-11604
688 (2002).

689 24. De Leo, A. *et al.* LANA oligomeric architecture is essential for KSHV nuclear body
690 formation and viral genome maintenance during latency. *PLoS Pathog* **15**,
691 e1007489 (2019).
692 25. Davis, Z.H. *et al.* Global mapping of herpesvirus-host protein complexes reveals
693 a transcription strategy for late genes. *Mol Cell* **57**, 349-360 (2015).
694 26. Hu, J., Liu, E. & Renne, R. Involvement of SSRP1 in latent replication of Kaposi's
695 sarcoma-associated herpesvirus. *J Virol* **83**, 11051-11063 (2009).
696 27. Banaszynski, L.A. *et al.* Hira-dependent histone H3.3 deposition facilitates PRC2
697 recruitment at developmental loci in ES cells. *Cell* **155**, 107-120 (2013).
698 28. Vladimirova, O. *et al.* Phase separation and DAXX redistribution contribute to
699 LANA nuclear body and KSHV genome dynamics during latency and
700 reactivation. *PLoS Pathog* **17**, e1009231 (2021).
701 29. Gunther, T. & Grundhoff, A. The epigenetic landscape of latent Kaposi sarcoma-
702 associated herpesvirus genomes. *PLoS Pathog* **6**, e1000935 (2010).
703 30. Krishnan, H.H. *et al.* Concurrent expression of latent and a limited number of lytic
704 genes with immune modulation and antiapoptotic function by Kaposi's sarcoma-
705 associated herpesvirus early during infection of primary endothelial and fibroblast
706 cells and subsequent decline of lytic gene expression. *J Virol* **78**, 3601-3620
707 (2004).
708 31. Murakami, Y. *et al.* Ets-1-dependent expression of vascular endothelial growth
709 factor receptors is activated by latency-associated nuclear antigen of Kaposi's
710 sarcoma-associated herpesvirus through interaction with Daxx. *J Biol Chem* **281**,
711 28113-28121 (2006).
712 32. Scherer, M. & Stamminger, T. Emerging Role of PML Nuclear Bodies in Innate
713 Immune Signaling. *J Virol* **90**, 5850-5854 (2016).
714 33. Scherer, M. *et al.* Dual signaling via interferon and DNA damage response elicits
715 entrapment by giant PML nuclear bodies. *Elife* **11** (2022).
716 34. Everett, R.D. & Maul, G.G. HSV-1 IE protein Vmw110 causes redistribution of
717 PML. *EMBO J* **13**, 5062-5069 (1994).
718 35. Ishov, A.M. & Maul, G.G. The periphery of nuclear domain 10 (ND10) as site of
719 DNA virus deposition. *J Cell Biol* **134**, 815-826 (1996).
720 36. Everett, R.D. *et al.* The disruption of ND10 during herpes simplex virus infection
721 correlates with the Vmw110- and proteasome-dependent loss of several PML
722 isoforms. *J Virol* **72**, 6581-6591 (1998).
723 37. Kim, Y.E. *et al.* Human cytomegalovirus infection causes degradation of Sp100
724 proteins that suppress viral gene expression. *J Virol* **85**, 11928-11937 (2011).
725 38. Berscheminski, J., Groitl, P., Dobner, T., Wimmer, P. & Schreiner, S. The
726 adenoviral oncogene E1A-13S interacts with a specific isoform of the tumor
727 suppressor PML to enhance viral transcription. *J Virol* **87**, 965-977 (2013).
728 39. Kedes, D.H., Lagunoff, M., Renne, R. & Ganem, D. Identification of the gene
729 encoding the major latency-associated nuclear antigen of the Kaposi's sarcoma-
730 associated herpesvirus. *J Clin Invest* **100**, 2606-2610 (1997).
731 40. Garber, A.C., Shu, M.A., Hu, J. & Renne, R. DNA binding and modulation of gene
732 expression by the latency-associated nuclear antigen of Kaposi's sarcoma-
733 associated herpesvirus. *J Virol* **75**, 7882-7892 (2001).

41. Li, P. *et al.* Phase transitions in the assembly of multivalent signalling proteins. *Nature* **483**, 336-340 (2012).
42. Cong, L. *et al.* Multiplex genome engineering using CRISPR/Cas systems. *Science* **339**, 819-823 (2013).
43. Mali, P. *et al.* RNA-guided human genome engineering via Cas9. *Science* **339**, 823-826 (2013).
44. Skene, P.J. & Henikoff, S. An efficient targeted nuclease strategy for high-resolution mapping of DNA binding sites. *Elife* **6** (2017).
45. Gunther, T. *et al.* A comparative epigenome analysis of gammaherpesviruses suggests cis-acting sequence features as critical mediators of rapid polycomb recruitment. *PLoS Pathog* **15**, e1007838 (2019).
46. Cai, Q. *et al.* A unique SUMO-2-interacting motif within LANA is essential for KSHV latency. *PLoS Pathog* **9**, e1003750 (2013).
47. Sahin, U. *et al.* Oxidative stress-induced assembly of PML nuclear bodies controls sumoylation of partner proteins. *J Cell Biol* **204**, 931-945 (2014).
48. Lin, D.Y. *et al.* Role of SUMO-interacting motif in Daxx SUMO modification, subnuclear localization, and repression of sumoylated transcription factors. *Mol Cell* **24**, 341-354 (2006).
49. Shih, H.M., Chang, C.C., Kuo, H.Y. & Lin, D.Y. Daxx mediates SUMO-dependent transcriptional control and subnuclear compartmentalization. *Biochem Soc Trans* **35**, 1397-1400 (2007).
50. Rai, T.S. *et al.* Histone chaperone HIRA deposits histone H3.3 onto foreign viral DNA and contributes to anti-viral intrinsic immunity. *Nucleic Acids Res* **45**, 11673-11683 (2017).
51. Morozov, V.M. *et al.* HIRA-mediated loading of histone variant H3.3 controls androgen-induced transcription by regulation of AR/BRD4 complex assembly at enhancers. *Nucleic Acids Res* **51**, 10194-10217 (2023).
52. Renne, R. *et al.* Lytic growth of Kaposi's sarcoma-associated herpesvirus (human herpesvirus 8) in culture. *Nat Med* **2**, 342-346 (1996).
53. Placek, B.J. *et al.* The histone variant H3.3 regulates gene expression during lytic infection with herpes simplex virus type 1. *J Virol* **83**, 1416-1421 (2009).
54. Ishov, A.M., Vladimirova, O.V. & Maul, G.G. Heterochromatin and ND10 are cell-cycle regulated and phosphorylation-dependent alternate nuclear sites of the transcription repressor Daxx and SWI/SNF protein ATRX. *J Cell Sci* **117**, 3807-3820 (2004).
55. Giovinazzi, S. *et al.* Regulation of mitosis and taxane response by Daxx and Rassf1. *Oncogene* **31**, 13-26 (2012).
56. Myoung, J. & Ganem, D. Generation of a doxycycline-inducible KSHV producer cell line of endothelial origin: maintenance of tight latency with efficient reactivation upon induction. *J Virol Methods* **174**, 12-21 (2011).
57. Brulois, K.F. *et al.* Construction and manipulation of a new Kaposi's sarcoma-associated herpesvirus bacterial artificial chromosome clone. *J Virol* **86**, 9708-9720 (2012).
58. Vieira, J. & O'Hearn, P.M. Use of the red fluorescent protein as a marker of Kaposi's sarcoma-associated herpesvirus lytic gene expression. *Virology* **325**, 225-240 (2004).

780 59. Renne, R. *et al.* Modulation of cellular and viral gene expression by the latency-
781 associated nuclear antigen of Kaposi's sarcoma-associated herpesvirus. *J Virol*
782 **75**, 458-468 (2001).
783 60. Ishov, A.M., Stenberg, R.M. & Maul, G.G. Human cytomegalovirus immediate
784 early interaction with host nuclear structures: definition of an immediate transcript
785 environment. *J Cell Biol* **138**, 5-16 (1997).
786 61. Orlando, D.A. *et al.* Quantitative ChIP-Seq normalization reveals global
787 modulation of the epigenome. *Cell Rep* **9**, 1163-1170 (2014).

788

A

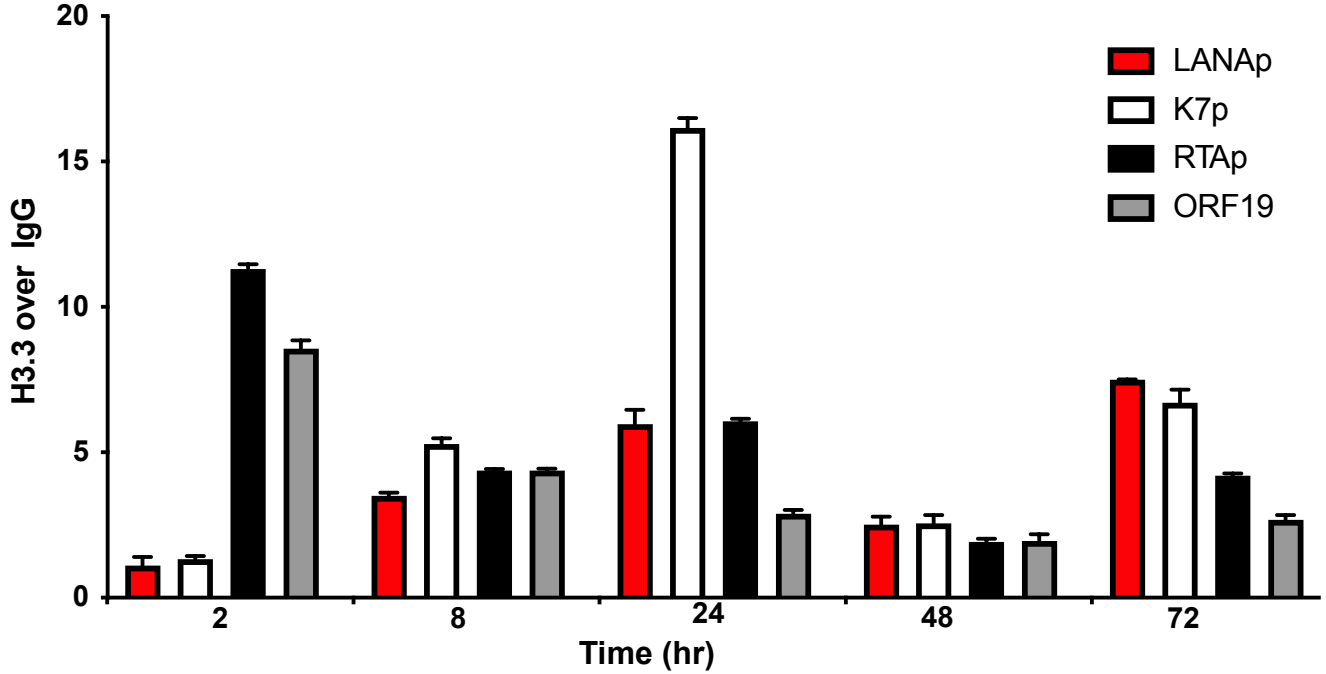
20
15
10
5
0
H3.3 over IgG
LANAp
K7p
RTAp
ORF19
2
8
24
48
72
Time (hr)

B

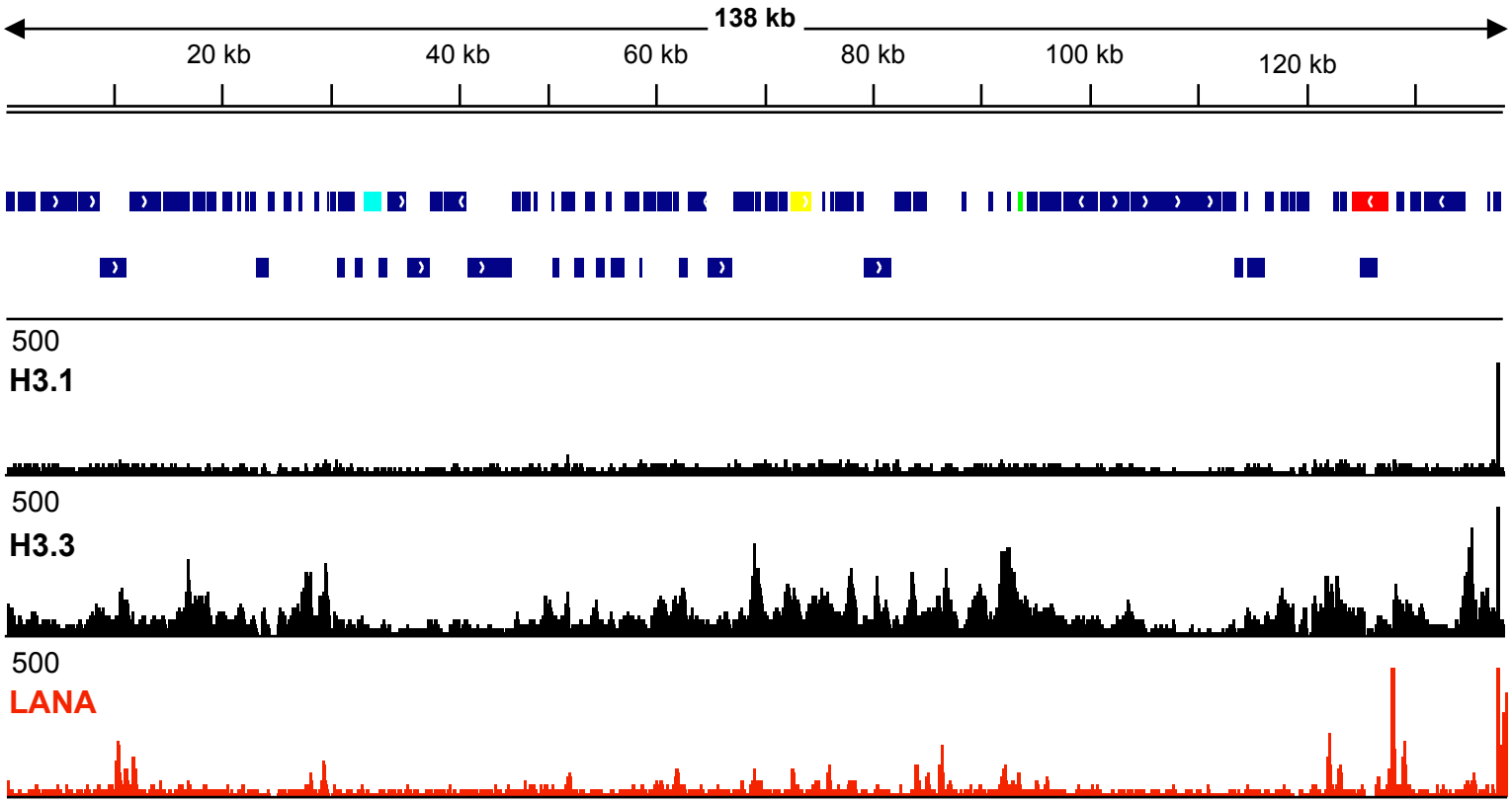
138 kb
20 kb
40 kb
60 kb
80 kb
100 kb
120 kb
500
H3.1
500
H3.3
500
LANA

A

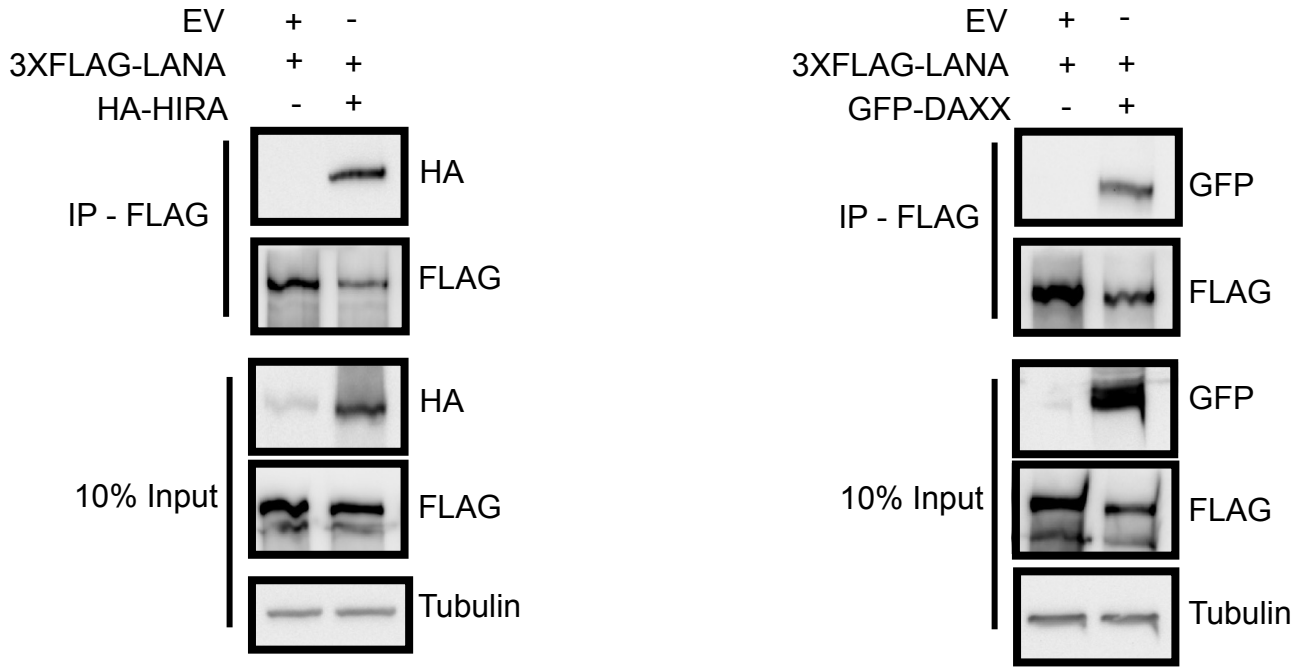
EV + -
3XFLAG-LANA + +
HA-HIRA - +
IP - FLAG
HA
FLAG
10% Input
HA
FLAG
Tubulin
EV + -
3XFLAG-LANA + +
GFP-DAXX - +
IP - FLAG
GFP
FLAG
10% Input
GFP
FLAG
Tubulin

B

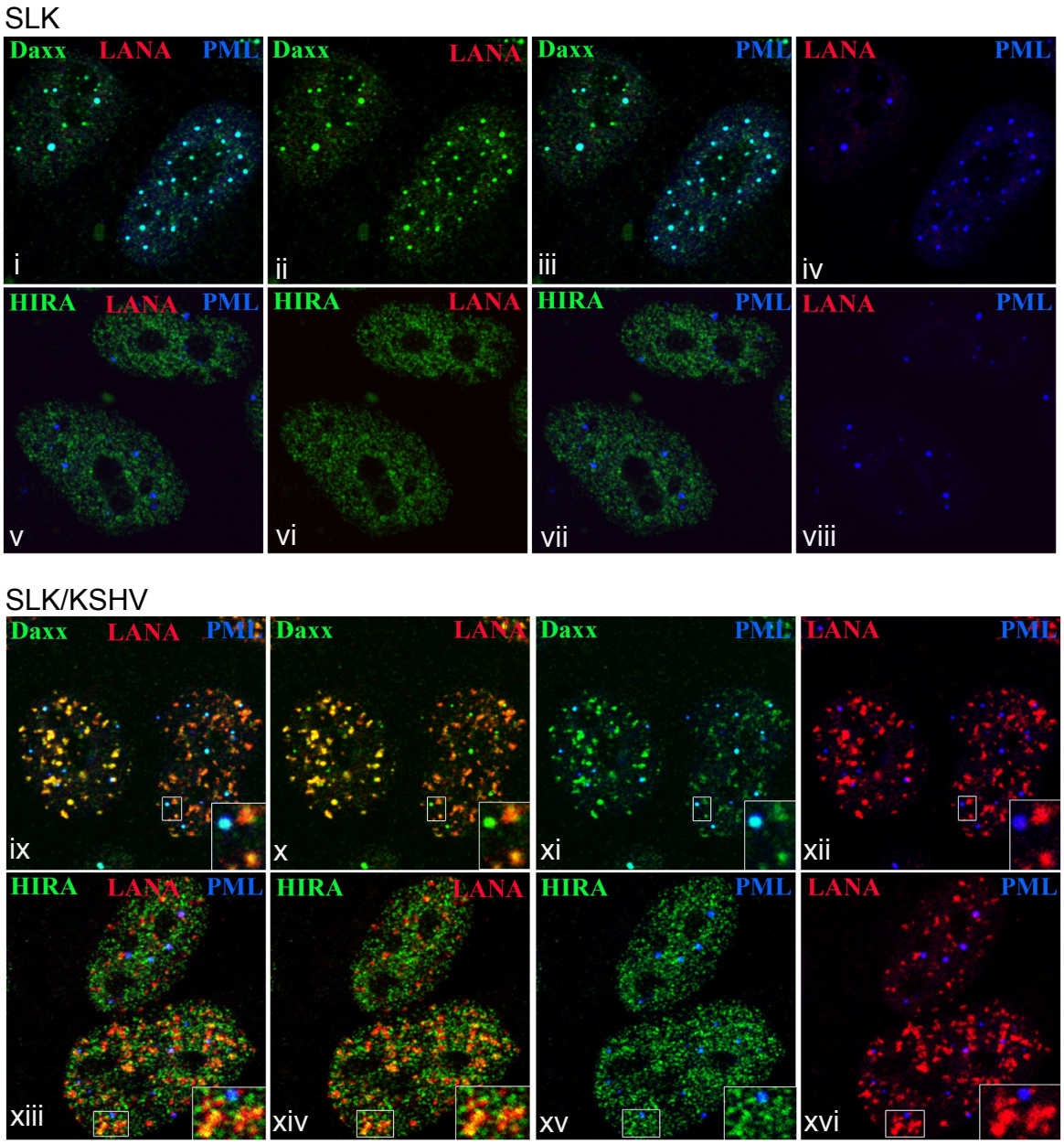
SLK
Daxx LANA PML
i
Daxx LANA
ii
Daxx PML
iii
LANA PML
iv
HIRA LANA PML
v
HIRA LANA
vi
HIRA PML
vii
LANA PML
viii
SLK/KSHV
Daxx LANA PML
ix
Daxx LANA
x
Daxx PML
xi
LANA PML
xii
HIRA LANA PML
xiii
HIRA LANA
xiv
HIRA PML
xv
LANA PML
xvi

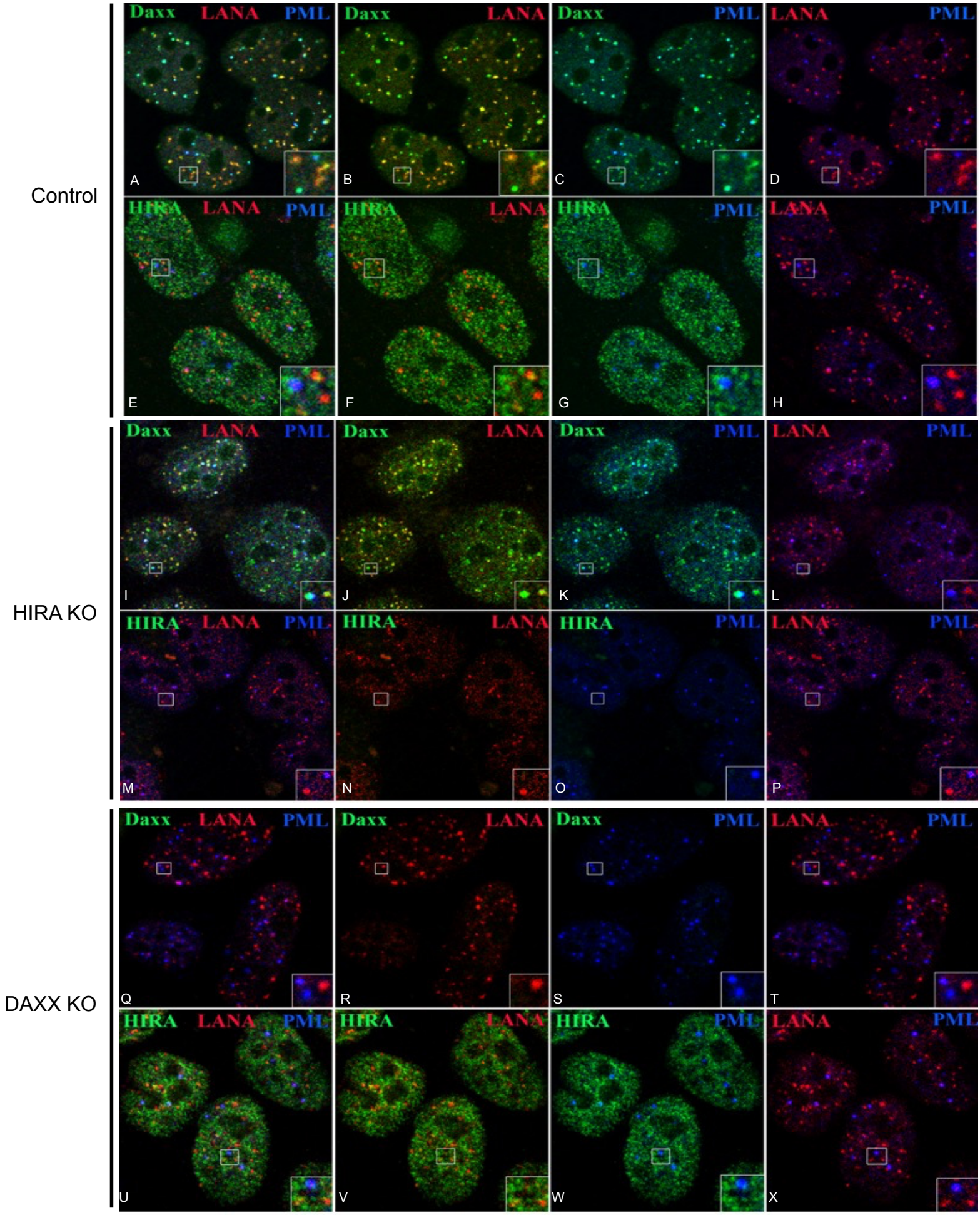
Control
HIRA KO
DAXX KO
Daxx LANA PML
HIRA LANA PML
A
B
C
D
E
F
G
H
I
J
K
L
M
N
O
P
Q
R
S
T
U
V
W
X

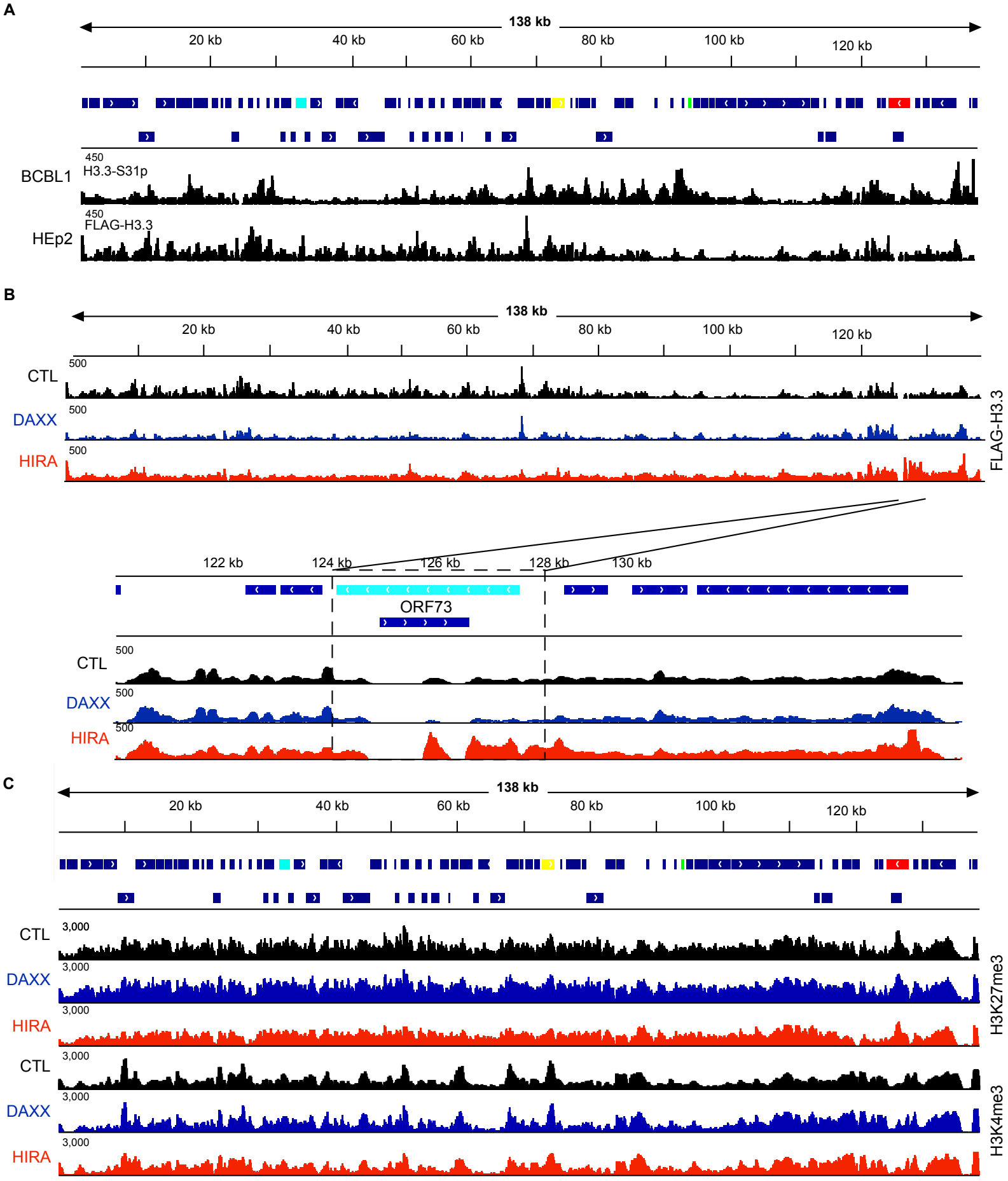
A
138 kb
20 kb
40 kb
60 kb
80 kb
100 kb
120 kb
BCBL1
450
H3.3-S31p
HEp2
450
FLAG-H3.3
B
138 kb
20 kb
40 kb
60 kb
80 kb
100 kb
120 kb
CTL
500
DAXX
500
HIRA
500
FLAG-H3.3
122 kb
124 kb
126 kb
128 kb
130 kb
ORF73
CTL
500
DAXX
500
HIRA
500
C
138 kb
20 kb
40 kb
60 kb
80 kb
100 kb
120 kb
CTL
3,000
DAXX
3,000
HIRA
3,000
H3K27me3
CTL
3,000
DAXX
3,000
HIRA
3,000
H3K4me3

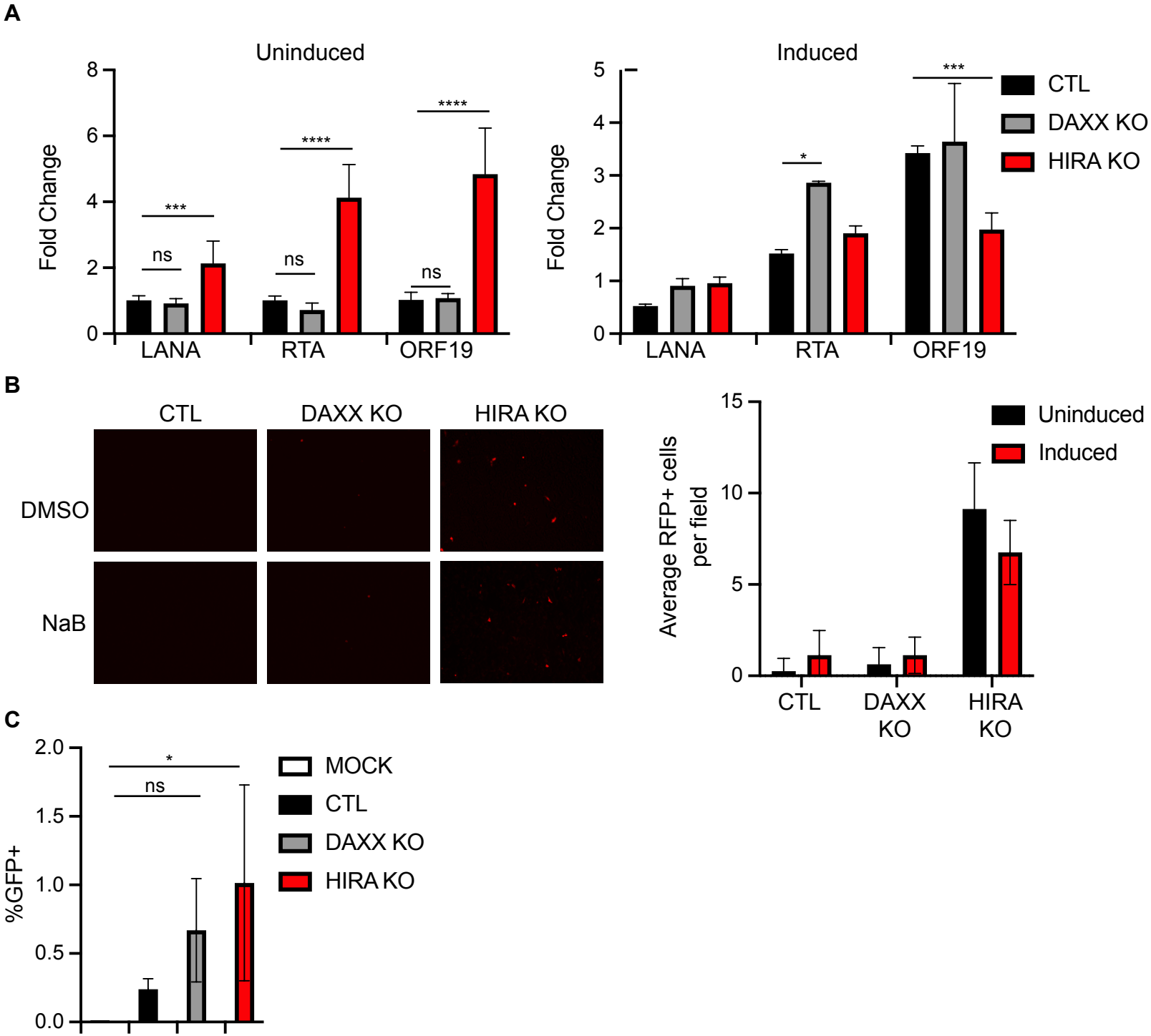
A
Uninduced
Induced
Fold Change
8
6
4
2
0
5
4
3
2
1
0
***
****
****
ns
ns
ns
*
***
LANA
RTA
ORF19
CTL
DAXX KO
HIRA KO
B
CTL
DAXX KO
HIRA KO
DMSO
NaB
Average RFP+ cells per field
15
10
5
0
Uninduced
Induced
CTL
DAXX KO
HIRA KO
C
%GFP+
2.0
1.5
1.0
0.5
0.0
*
ns
MOCK
CTL
DAXX KO
HIRA KO